Applied Catalysis B: Environmental 267 (2020) 118608

Contents lists available at ScienceDirect

Applied Catalysis B: Environmental

journal homepage: www.elsevier.com/locate/apcatb

Manganese oxide-based porous electrodes for rapid and selective (electro) catalytic removal and recovery of sulfide from wastewater

Natalia Sergienko[a,b], Jelena Radjenovic[a,c,*]

[a] Catalan Institute for Water Research (ICRA), c/Emili Grahit 101, 17003 Girona, Spain
[b] University of Girona, Girona, Spain
[c] Catalan Institution for Research and Advanced Studies (ICREA), Passeig Lluís Companys 23, 08010 Barcelona, Spain

ARTICLE INFO

Keywords:
sulfide oxidation
manganese oxide
heterogeneous catalysis
electrocatalytic oxidation
sulfur recovery

ABSTRACT

Sulfide and its removal is a major concern in wastewater treatment as it represents a threat to human health and the structural integrity of the water distribution system. In this study, we demonstrated for the first time an exceptional performance of manganese oxide-coated graphite felt (GF-Mn_xO_y) electrodes for selective sulfide oxidation to sulfur. Oxidation state, loading, morphology and crystallinity of Mn_xO_y coating was tuned using electrodeposition synthesis method to enable an efficient and selective sulfide oxidation to sulfur. Excellent (electro)catalytic activity of GF-Mn_xO_y yielded up to 25-fold increase in sulfide removal rates compared to pristine GF, both in the open circuit (OC, no applied potential) and under anodic polarization at 0.4 V vs Standard Hydrogen Electrode (SHE). Although anodic polarization did not further enhance sulfide oxidation rate compared to OC, it enabled a continuous re-oxidation of the reduced Mn_xO_y coating after its reaction with sulfide. Thus, restoring of the catalytic properties of Mn_xO_y coating enabled higher sulfide removal rates compared with the OC experiment. The formed elemental sulfur remained at the surface of GF-Mn_xO_y leading to a gradual electrode passivation. The deposited sulfur was successfully dissolved by reversing the polarity of the GF-Mn_xO_y electrode to -0.8 V vs SHE. However, full electrode recovery and restoring of the initial sulfide removal rates could not be achieved as cathodic polarization at -0.8 V vs SHE during longer time (> 3 hours) required to remove S^0 also caused a partial dissolution of the Mn_xO_y coating. (Electro)catalytic sulfide removal was somewhat decreased in real sewage (2.42 ± 0.02 h^{-1} vs 0.93 ± 0.15 h^{-1} in $NaNO_3$ supporting electrolyte and real sewage, respectively). The selectivity of the process towards deposition of elemental sulfur was decreased in real sewage due to partial production of colloidal sulfur, which was presumably caused by diffusion limitation imposed by presence of other ions. Due to lesser extend of GF-Mn_2O_3 electrode passivation in real sewage, sulfide removal rates remained stable over six subsequent application cycles. In summary, Mn_xO_y-based electrodes demonstrated exceptional (electro)catalytic activity and selectivity for sulfide oxidation to sulfur and thus its complete separation from water. Upscaling of the proposed electrochemical system and its application for the treatment of complex wastewater streams requires further efforts to maintain the selectivity towards deposited sulfur as a final product and allow its complete recovery.

1. Introduction

Sulfide is a toxic, colorless gas with characteristic rotten egg smell, that is generated in wastewater systems by sulfate reducing bacteria (SRB) [1]. SRB anaerobic respiration is particularly favored by the abundance of sulfate that is introduced into wastewater collection systems with household cleaning detergents. Beyond its malodor, sulfide represents a serious threat to the structural integrity of the sewers. For example, only in Germany the costs of concrete sewers replacement due to corrosion caused by sulfide was estimated at €100 million per year [2].

Traditional approach for sulfide control in wastewater collection system based on the addition of chemicals. is associated with high operating costs and formation of toxic metal-containing sludge in the case of precipitation methods, or sulfide reformation at the end of the pipeline in the case of oxidation methods [3]. Electrochemical approach for sulfide control is gaining more attention nowadays as it offers robust *in situ* sulfide removal while avoiding costs associated with the production, transportation and handling of chemicals. Besides that, a number of studies demonstrated that sulfide can be selectively oxidized

* Corresponding author at: Catalan Institute for Water Research (ICRA), Scientific and Technological Park of the University of Girona, 17003 Girona, Spain
E-mail address: jradjenovic@icra.cat (J. Radjenovic).

https://doi.org/10.1016/j.apcatb.2020.118608
Received 25 September 2019; Received in revised form 12 December 2019; Accepted 6 January 2020
Available online 01 February 2020

to elemental sulfur directly at the electrode surface, which avoids sulfide reformation and formation of toxic sludge [3].

The choice of the appropriate electrode material is especially important for the direct oxidation process. It was demonstrated that low-cost carbon-based materials, characterized by a high surface area and low resistance, are capable of efficient electrochemical sulfide oxidation to elemental sulfur [4–7]. However, their performance can be enhanced even further through material modification with a catalyst active towards oxidation of hydrogen sulfide.

Manganese oxide (Mn_xO_y) -coated electrodes are widely applied in the field of batteries and supercapacitors due to their high capacitance and ability to exist in different oxidation states [8]. This possibility of easy and reversible transition between different oxidation states, Mn (II), Mn(III) and Mn(IV), enables Mn_xO_y to participate in a wide range of oxidation and reduction reactions, making it a versatile catalyst [9–11]. Although Mn_xO_y-coated electrodes have been extensively investigated and applied in the energy field [12], only a few studies have explored environmental applications of these materials for water treatment. For example, several studies reported that Mn_xO_y nanostructures are capable of efficient elelctrooxidation of refractory organics, such as aniline [13], formaldehyde [14,15], phenol [16–18] with its derivatives [19–21] and low molecular weight organic acids [22,23] as well as some volatile organic contaminants [24,25]. Besides that morphological characteristics of certain Mn_xO_y forms achieve efficient adsorption of metals from wastewater by retaining ions inside Mn_xO_y three-dimensional network [26–28].

Ability of manganese oxide to oxidize sulfide was previously studied as a natural process that occurs in sediments [29]. For example, Herszage et al. reported that manganese mineral oxides present in freshwater sediments are capable of robust sulfide oxidation with elemental sulfur or sulfate as a reaction product depending on the local pH [30]. However, high affinity of manganese oxides towards sulfide oxidation was never exploited in wastewater treatment. Some studies proposed sulfide oxidation with potassium permanganate, which yields fast sulfide removal but is also inherently limited by the gradual depletion of the catalyst and formation of a precipitant [31–33]. Besides that, the presence of dissolved manganese ions is not desirable since it compromises the quality of the treated water [34].

Over the years, a diverse range of Mn_xO_y-based electrode synthesis routes was developed, including electrodeposition [35], chemical oxidation [36], hydrothermal [37] or solvothermal methods [38], sol-gel [39] and pulsed-laser deposition [40]. Electrodeposition method is particularly attractive as it allows a morphology-controlled growth of the Mn_xO_y coating through variation of different parameters such as precursor type and concentration, composition of electrolyte, potential and time [35,41,42]. Optimization of the electrodeposition parameters is of high importance in the synthesis of the Mn_xO_y coating as it determines the activity of the produced material towards the desired reaction.

Here, we propose for the first time the use of Mn_xO_y-based electrodes in an electrochemical cell for sulfide removal via pathway, while achieving continuous regeneration of the Mn_xO_y catalytic coating with applied potential. The coating of electrochemically-deposited manganese oxides over a porous graphite felt (GF) was fine-tuned in terms of precursor concentration and loading to obtain specific Mn_xO_y oxidation state, loading, morphology and crystallinity and maximize its (electro) catalytic activity and selectivity towards sulfide oxidation to sulfur. Gradual loss of electrode performance due to the formation of the deposited sulfur was also addressed by the application of cathodic polarization for the dissolution of S^0. Furthermore, the synthesized GF-Mn_xO_y electrodes were employed for sulfide removal from real sewage to investigate the performance of Mn_xO_y-based electrodes in sulfide removal under realistic scenarios.

2. Material and methods

2.1. Mn_xO_y-coated electrode synthesis

GF-Mn_xO_y electrodes were synthesized using anodic electrodeposition technique. The synthesis was performed in a three-electrode setup at ambient temperature (i.e., 24 ± 1 °C), with GF (2 × 1.5 x 0.5 cm) obtained from Final Advanced Materials (France) as a working electrode (anode), carbon foil as counter electrode and Ag/AgCl (KCl 3 M, Bioanalytical systems, IN) as reference electrode. The electrodeposition medium contained 0.2 M $MnSO_4$ and 0.02 M H_2SO_4. To investigate the influence of the precursor concentration on the Mn_xO_y coating characteristics, electrodeposition synthesis was also performed using 0.02 M $MnSO_4$ and 0.02 M H_2SO_4. In all synthesis procedures, 0.01 vol % Triton X-100 was used to improve the deposition efficiency and obtain a more uniform coating on a porous structure of GF [42]. Deposition was performed in potentiostatic mode at + 1.63 V vs SHE. To ensure the reproducibility of each deposition, the mass of the manganese oxide loading was calculated according to Faraday's law and the charge was limited to 200 C or 1000 C. After completion of the synthesis process, material was rinsed thoroughly with distilled water. To ensure complete removal of Triton X-100, synthesized material was treated with isopropanol (IPA) at 60 °C for 15 min, followed by the second rinsing with distilled water. To investigate the effect of temperature treatment, samples were calcinated at 300, 400 and 500 °C in air for 1 h in a tubular oven (Nabertherm, Germany). "H" in the sample code stands for high precursor concentration (i.e., 0.2 M $MnSO_4$), while "L" means low precursor concentration (i.e., 0.02 M $MnSO_4$). The amount of charge (i.e., 200 C or 1000 C) is also mentioned in the code. Names of samples, which were subjected to temperature treatment include "c".

2.2. Material characterization

The surface morphology of the synthesized materials was examined using an ultra-high-resolution field emission scanning electron microscopy (SEM) (The Magellan 400 L, FEI, US). The crystal structure of the GF-Mn_xO_y electrodes was determined by an X-ray powder diffractometer (X'Pert MPD, PANalytical, Netherlands) with Cu as Kα radiation source. The X-ray diffraction (XRD) patterns of the samples were recorded between 10 and 80º (2 h) at a scan step size of 0.02º, and a time per step of 353 s. Chemical state analysis of Mn_xO_y coating was performed with X-ray photoelectron spectroscopy (XPS) using an X-ray photoelectron spectrometer (PHOIBOS 150, Specs, Germany). All XPS spectra were calibrated using the C 1s peak at 284.6 eV. Mn 3s doublet peak separation values were then used to determine the valence state of Mn in the sample.

2.3. (Electro)catalytic sulfide removal and electrode regeneration tests

Electrochemical experiments were carried out in a glass cell (250 mL) with an air-tight seal. GF or GF-Mn_xO_y materials was used as an anode, Ag/AgCl (3 M KCl) as reference electrode and Pt coil was a counter electrode separated from the anodic compartment by a porous glass frit, to minimize the interference from the cathodic reactions. Electrochemical cell was purged with nitrogen prior to all experiments to minimize the loss of sulfide due to its reaction with the dissolved oxygen Experiments were performed in both OC and under constant potential of + 0.4 V vs SHE to evaluate sulfide removal using GF and the synthesized GF-Mn_xO_y electrodes. The initial concentration of sulfide was 2.7 mM, with 2.6 mM $NaNO_3$ as a supporting electrolyte (conductivity 3 – 3.2 mS cm^{-1}, pH 8.2). pH of the supporting electrolyte was maintained at pH 8-8.2 during the 2 hours experiments to avoid sulfide stripping. Cathodic regeneration of the sulfur loaded electrodes was performed in the same reactor as described above under constant potential of -0.8 V vs SHE and in a 10 mM $NaNO_3$ electrolyte (conductivity of 3-3.2 mS cm^{-1}). All experiments were performed in duplicates and

values are expressed as mean with their standard errors.

To investigate the performance of Mn_xO_y-coated electrodes in sulfide removal under realistic conditions, experiments were performed with real sewage that was deoxygenated and amended with the same initial concentration of sulfide (i.e., 2.7 mM) and adjusted to pH 8.2. The conductivity of the sampled sewage was identical to the supporting electrolyte used in the experiments (i.e., 3.2 mS cm^{-1}).

2.4. Sample analysis

Chemical oxygen demand (COD) and free chlorine were measured using LCK test cuvette method (HACH, US). Concentration of total dissolved manganese and other metals in $NaNO_3$ supporting electrolyte and sewage was measured by means of plasma optical emission spectrometry (ICP-OES) (Agilent 5100, Agilent Technologies, US), to evaluate the stability of the Mn_xO_y coating. The concentration of dissolved sulfur species (i.e., $HS-$, $S_2O_3^{2-}$, SO_4^{2-}) was determined by ion chromatography (IC), using a Dionex IC5000 (Dionex, USA). Although several attempts were made to determine the concentration of the formed polysulfides, none of the methods reported in literature was found to be reliable. For example, previous study applied oxidation of all dissolved sulfur species to sulfate with H_2O_2 at high pH as a technique to determine the formed polysulfides [43]. However, in our study the main product of such reaction was colloidal sulfur, which cannot be determined with ion chromatography [44]. Therefore, the presence of polysulfides could only be indicated by the gradual appearance of characteristic yellow color and also higher concentrations of the soluble sulfur species, end products of further polysulfide oxidation [45]. In the experiments where the electrolyte solution stayed colorless throughout the experiment, the difference between the total sulfide added and the dissolved sulfur species measured was assumed to be electrodeposited elemental sulfur. Measured sulfide concentrations were normalized against the initial values, and the data from the duplicate experiments were then fitted with a first-order kinetic relationship.

3. Results and discussion

3.1. Characterization of GF-Mn_xO_y electrodes

Fig. 1 represents XRD patterns of the synthesized GF-Mn_xO_y materials. As expected, XRD spectra of the non-calcinated samples did not show any peak that could be attributed to a crystalline phase of Mn_xO_y, meaning that electrodeposition itself results in a completely amorphous coating. On the contrary, all calcinated sample showed signals characteristic of an orthorhombic bixbyite crystalline phase, α-Mn_2O_3 (Mn III) (Fig. 1a, Figure S2). As can be concluded from the improved signal,

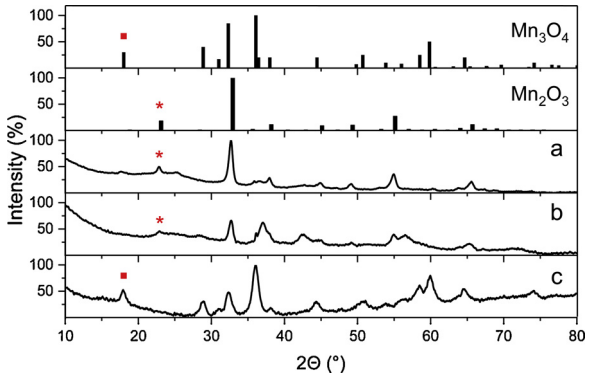

Fig. 1. XRD patterns of GF-Mn_xO_y electrodes obtained using different precursor concentrations (i.e., 0.02 M (L) and 0.2 M $MnSO_4$ (H)), electrical charge applied (200 C and 1000 C), followed by the calcination step: a) L-200 C, c., b) H-200 C, c., and c) H-1000 C, c. Reference patterns are depicted at the top for Mn_3O_4 (■), α-Mn_2O_3 (*), where the symbols indicate the respective low-angle reflections.

Table 1
XPS peak analyses of GF-Mn_xO_y electrodes obtained using different precursor concentrations (i.e., 0.02 M and 0.2 M $MnSO_4$), electrical charge applied (200 C and 1000 C), and with and without the calcination step. The deconvoluted data are shown for the Mn 2p3/2, Mn 3s and O 1s spectra.

Sample	Mn $2p_{3/2}$, E_b, eV	Mn 3 s			n[e]
		E_b (1), eV	E_b (2), eV	ΔE, eV	
L-200C	642	88.3	83.7	4.6	4
L-200C, c.	642	89.1	83.9	5.2	3
H-200C	641.9	88.8	84.2	4.6	4
H-200C, c.	641.7	89	83.8	5.2	3
H-1000C	641.9	88.4	84.1	4.3	4
H-1000C, c.	641.6	88.9	83.7	5.2	3

increase of calcination temperature improved the crystallinity of the material. The same oxide type was obtained in the samples synthesized at higher precursor concentration (Fig. 1b). Sample in which the Mn_xO_y loading was increased to 1000 C demonstrated a pattern more typical of tetragonal hausmannite, Mn_3O_4, comprised of Mn with two valence states: Mn(III) and Mn(II) (Fig. 1c). The appearance of Mn(II) can be caused by an increased thickness of the coating obtained by the longer time of the electrodeposition. Deeper layers of such coating are completely isolated from oxygen during the calcination step, thus leading to Mn_xO_y thermal reduction to lower oxide forms such as Mn(II) [46].

XPS analysis was also carried out to investigate the surface composition of the amorphous Mn_xO_y coating and to compliment the XRD analysis results of the crystalline samples. Mn valence state was determined based on the Mn 3 s doublet peak separation as a more reliable method compared to the one based on the location of Mn 2p peaks only [42]. Different Mn 3 s doublet peak splitting values were previously reported in literature including 4.5, 5.2, 5.4, and 5.8 eV for MnO_2 (Mn I), Mn_2O_3 (Mn III), Mn_3O_4 (Mn II, Mn III), and MnO (Mn II), respectively [42,47,48]. As can be seen from Table 1, doublet peak separation values for all samples that were not subjected to calcination (i.e., L-200 C.; H-200 C.; H-1000 C.) are in the range common for MnO_2 (Mn IV). This valence state is typical for Mn-based coatings synthesized via anodic electrodeposition pathway, and forms via the following reaction [49]:

$$Mn^{2+} + 4OH^- \rightarrow MnO_2 + 2H_2O + 2e^- \quad (1)$$

Doublet peak separation increased for calcinated samples (i.e., L-200 C, c.; H-200 C, c.; H-1000 C, c.) indicating the transformation of MnO_2 (Mn IV) into Mn_2O_3 (Mn III), which goes in agreement with the XRD data. This phase transformation took place due to the thermal decomposition of MnO_2 at 500 °C according to the following reaction [46,50]:

$$4MnO_2 \rightarrow 2Mn_2O_3 + O_2 \quad (2)$$

The dominant surface species for samples with the higher Mn-loading (i.e., 1000 C) was also Mn_2O_3, confirming the assumption that Mn(II) is mainly present in the inner layers of the coating.

Fig. 2 and Figure S1 compare the morphology of various Mn_xO_y coatings prepared under different electrodeposition parameters. Mn_xO_y coating synthesized at higher $MnSO_4$ concentration (i.e., 0.2 M) has nanorod-like morphology (Fig. 2c, d). When the charge was increased (Fig. 2e, f), the electrode coating became thicker and smoother as nanorods became less pronounced, merging into each other and forming a dense layer. The observed morphological difference can be explained through the mechanism of Mn_xO_y layer formation. Manganese oxide coating formation using electrodeposition is a complex process that can be divided into two main steps: *i)* nuclei formation, and *ii)* crystal growth [51]. Nuclei formation and continuous uptake of new substrate sites normally occurs within seconds in the initial stage of electrodeposition, resulting in a very rough coating with high specific surface area. As the electrodeposition continues, the formed nuclei continue to

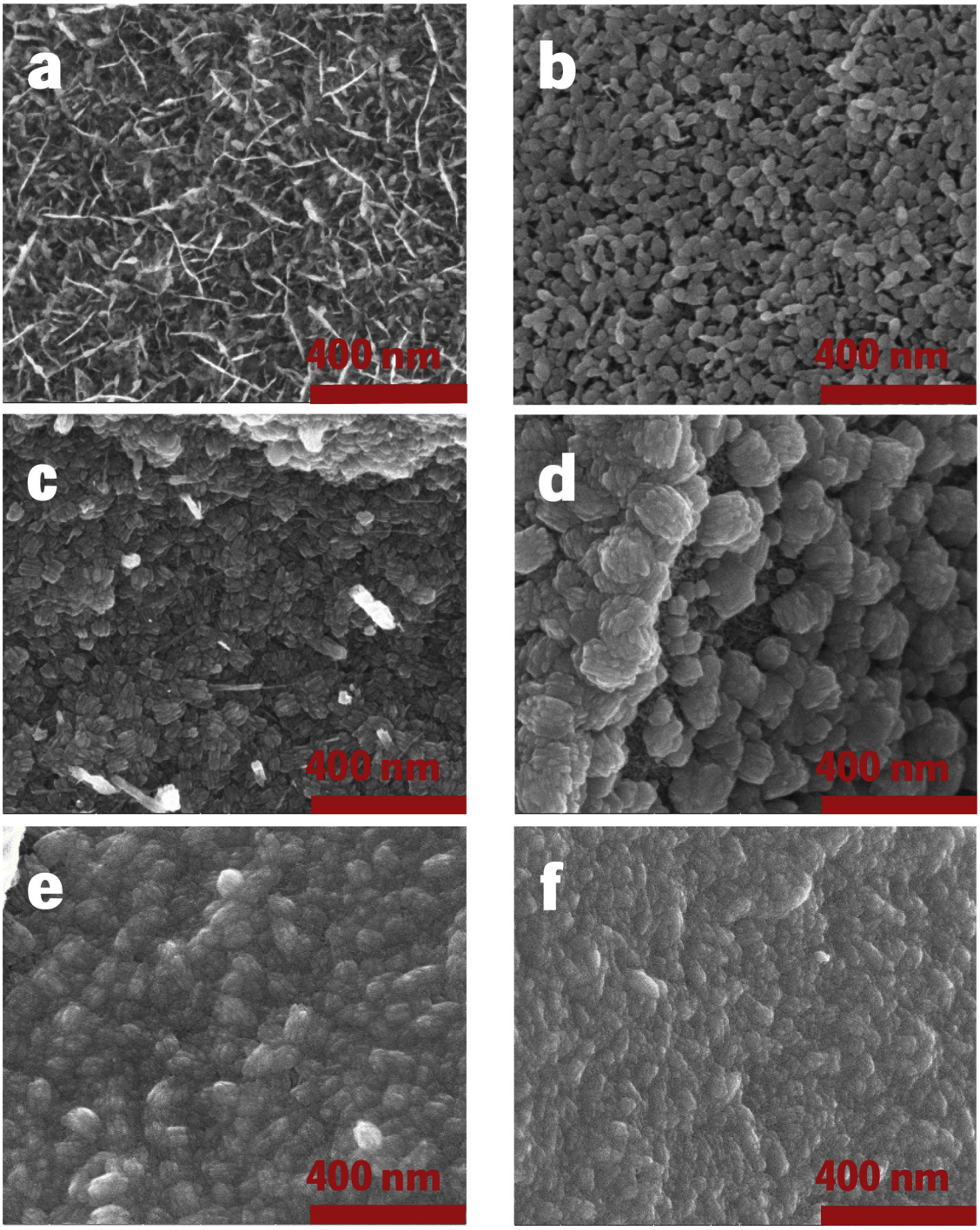

Fig. 2. SEM images of GF-Mn_xO_y electrodes synthesized using different electrodeposition conditions and protocols: a) L-200 C, b) L-200 C, c., c) H-200 C, d) H-200 C, c., e) H-1000 C, and f) H-1000 C, c.

grow in all directions and finally merge into adjacent growth centers, forming Mn_xO_y film over the entire GF substrate surface. Formation of new nuclei during continuous crystal growth also occurs, however, this process takes place on the top of the existing Mn_xO_y layer. Thus, Mn_xO_y layer becomes thicker and smoother, while specific surface area of the coating decreases due to the presence of less relief in its structure. Mn_xO_y coating obtained at lower precursor concentrations (i.e., 0.02 M $MnSO_4$) is characterized by a nanoneedle-like structure mixed with nanorods of smaller size compared to the samples synthesized at higher precursor concentration (Fig. 2a). According to Babakhani et al., instantaneous mechanism can be suppressed by limiting Mn^{2+} concentration at the electrode surface, which yields material with more compact grains (Fig. 2a, b) [49]. Calcination did not have any significant effect on the morphology of the synthesized materials.

3.2. Catalytic activity of GF-Mn_xO_y electrodes towards sulfide oxidation

First, catalytic activity of each synthesized material was evaluated in the OC experiments. All electrode materials synthesized demonstrated remarkable catalytic activity of Mn_xO_y coating towards HS^- oxidation even in the absence of applied potential. More than 80% removal was achieved within two hours, while no sulfide removal was

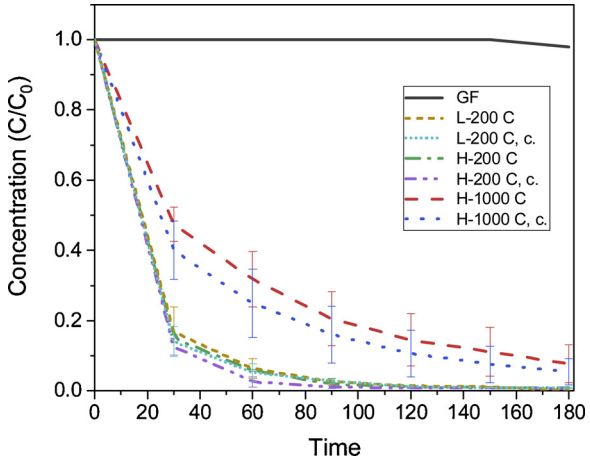

Fig. 3. Decrease in HS^- concentration (c) normalized to the initial value (c_0) over experiment time during the open circuit (OC) experiments using GF or GF-Mn_xO_y electrodes.

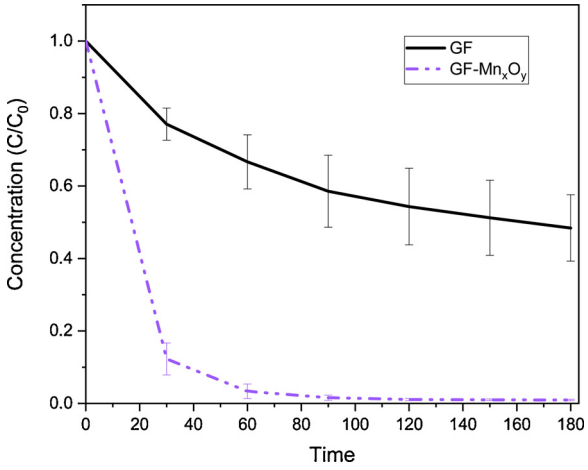

Fig. 4. HS^- removal rate at 0.4 V vs SHE applied to GF or GF-Mn_xO_y electrodes (H-200 C, c.).

observed when pristine GF was used in the OC experiments (Fig. 3). The main final product of HS^- oxidation was elemental sulfur, with more than 85% yield of S°. The presence of low concentrations of dissolved sulfur species such as thiosulfate and sulfate was also detected (up to 15% of the initial sulfide concentration). Elemental sulfur produced as a result of catalytic oxidation by Mn_xO_y coating remained at the electrode surface, as was confirmed by SEM images (Figure S5), EDX (Figure S6) and XPS.

Catalytic reaction between sulfide and manganese oxides starts with HS^- adsorption onto the catalyst surface. Adsorption is followed by the formation of a surface complex (Equation 3) and its subsequent oxidation at the surface (Equation 4,5) [30]. Electron transfer can occur in two consecutive steps or just in one step according to the valence state of the Mn catalyst:

$$Mn^{IV} + HS^- \rightleftharpoons Mn^{IV}S^- + H_2O \quad (3)$$

$$Mn^{IV}S^- \rightarrow Mn^{III}S \quad (4)$$

$$Mn^{III}\ S \rightarrow Mn^{II}S \quad (5)$$

$$Mn^{II}\ S \rightarrow Mn^{II} + S^0 \quad (6)$$

The reaction mechanism for non-calcinated samples includes one additional step compared to calcinated materials, but the transition between the surface complexes is so rapid, that it does not significantly affect removal rates (i.e., 1.83 ± 0.14 h^{-1} and 1.89 ± 0.01 h^{-1} for Mn (IV) and Mn(III), respectively) [52,53]. S° that is produced as a result of the reaction, can either undergo complexation to S^8 or migrate to the neighboring non-reduced Mn-oxide site, where it can get further oxidized to thiosulfate or sulfate and finally released into the solution [30]. Even though initial valence state of the Mn_xO_y catalyst had almost no effect on sulfide removal, the kinetics of the process for calcinated samples was slightly improved due to the more crystalline coating (Table S2).

While materials synthesized at high and low precursor concentrations (i.e., 0.2 M and 0.02 M $MnSO_4$) showed similar performance in terms of sulfide removal rates (i.e., 1.83 ± 0.14 h^{-1} and 1.74 ± 0.1 h^{-1}, respectively), increased charge loading significantly deteriorated the removal rates (Fig. 3). When the charge was increased from 200 C to 1000 C, sulfide removal rate decreased from 1.83 ± 0.14 h^{-1} h^{-1} to 0.63 ± 0.2 h^{-1} (Fig. 3). The performance of each synthesized material greatly depends on the active surface area of the Mn_xO_y coating. Even though the active surface area of the synthesized GF-Mn_xO_y electrodes could not be measured due the fibrous nature of the substrate, it decreases over the electrodeposition process with the nuclei growth, due to the evening out of the surface and less relief in its structure. Therefore, such Mn_xO_y films demonstrate worse performance as they lose active sites available for sulfide oxidation.

Prior to the application of GF-Mn_xO_y electrode for electrochemical sulfide oxidation at 0.4 V vs SHE, its stability under anodic polarization was verified by performing experiments at 0.4 V vs SHE, while measuring total dissolved manganese (Table S1). The obtained values after 3 and 6 h of anodic polarization showed that there was no release of manganese ions as into the electrolyte, thus the stability of the synthesized electrode was confirmed. As can be seen from Fig. 4, the presence of Mn_xO_y coating yielded eight-fold higher sulfide removal rate compared to GF (i.e., 1.83 ± 0.14 h^{-1} for GF-Mn_xO_y and 0.23 ± 0.12 h^{-1} for GF). However, in comparison with the OC experiments performed at GF-Mn_xO_y electrode, application of potential did not have any significant effect on the HS^- removal rate or the final products of the reaction (Figure S4). As was demonstrated by XPS, increase of Mn 3 s doublet peak separation of GF-Mn_xO_y electrodes applied for sulfide removal in the OC indicates the reduction of the catalytic coating from Mn(III) to Mn(II). Mn reduction also occurred when HS^- removal was performed at 0.4 V vs SHE, yet, partial recovery of the catalytic coating was achieved as both Mn(II) and Mn(III) were detected by the XPS analyses (Table 2). Therefore, when potential is applied, catalytic HS^- oxidation occurs simultaneously with the oxidation of the reduced Mn-oxide catalytic coating, which can be highly beneficial for the long-term application of such material.

3.3. Application of GF-Mn_2O_3 electrodes for sulfide removal and sulfur recovery

Repeated application of GF-Mn_2O_3 electrode (H-200 C, c.) in the OC experiment and at 0.4 V vs SHE was performed to investigate the impact of anodic potential application on the sulfide removal process (Fig. 5). As can be seen from Fig. 5a, first order removal rate in the OC

Table 2
XPS peak analysis of synthesized GF-Mn_xO_y electrode (H-200 C, c.), electrode used in the OC experiment and electrode used for electrochemical (EC) removal of sulfide at 0.4 V vs SHE, both performed in 2.7 mM HS^- and 2.6 mM $NaNO_3$ electrolyte, at pH 8-8.2. The deconvoluted data is shown for the Mn 2p3/2, Mn 3s and O 1s spectra.

Sample	Mn $2p_{3/2}$, E_b, eV	Mn 3 s			n[e]
		E_b (1), eV	E_b (2), eV	ΔE, eV	
pristine	641.7	89	83.8	5.2	3
after OC	641.9	89.3	83.5	5.8	2
after EC	641.7	89	83.6	5.4	2,3

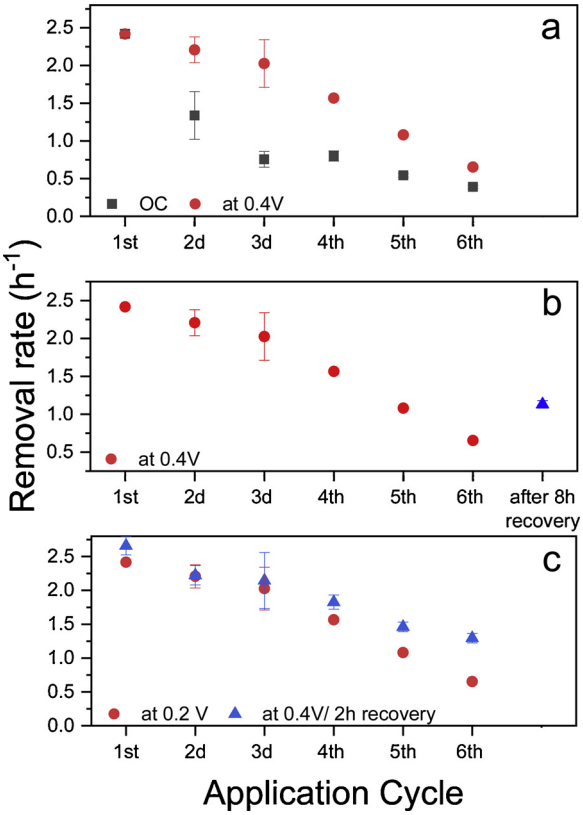

Fig. 5. Observed first-order sulfide removal rates (h^{-1}) at GF-Mn_xO_y electrodes (H-200 C, c.): a) in the OC experiment and at +0.4 V vs SHE of applied anode potential in six subsequent cycles, b) at +0.4 V vs SHE in repeated application with the last cycle preceded by 8 hours of cathodic recovery at -0.8 V vs SHE, c) at +0.4 V vs SHE in six subsequent application cycles, when each cycle was followed by 2 hours of cathodic recovery at -0.8 V vs SHE.

experiments was drastically decreased in each subsequent cycle, going down from 2.42 ± 0.05 h^{-1} in the first cycle to 0.39 ± 0.02 h^{-1} in the sixth cycle. The performance was partly lost due to the gradual depletion of the catalytically active Mn(III) sites and its substitution with reduced Mn(II). This loss of the catalytic activity of the coating can be counteracted by the application of low anodic potential, which oxidizes Mn(II) back to Mn(III). Indeed, when the experiments were performed at 0.4 V vs SHE, the performance of GF-Mn_2O_3 electrode was improved compared to the OC (i.e., 0.39 ± 0.02 h^{-1} and 0.65 ± 0.03 h^{-1} in the sixth cycle in the OC and at 0.4 V vs SHE, respectively). Significant decrease in the first order removal rate occurred after the fourth application both with and without the applied potential (i.e., 2.42 ± 0.05 h^{-1} in the first cycle to 1.57 ± 0.01 h^{-1} in the fourth cycle), indicating the electrode passivation with the electrodeposited elemental sulfur.

Gradual decrease in electrode performance is a common problem reported by many studies focused on direct electrochemical oxidation of HS^- [4,43,54]. The final product, elemental sulfur, has high electrical resistance (1017 Ω cm-1) [3], and its formation at the electrode surface limits the electron transfer and passivates the electrode. Electrodeposited elemental sulfur also imposes mass transfer limitations, which further aggravates the performance. Therefore, electrochemical sulfide oxidation and separation from the wastewater needs to be coupled with an appropriate strategy for elemental sulfur recovery. Several studies [4,55] successfully applied cathodic polarization for electrochemical dissolution of sulfur and its recovery in the form of sulfide. The recovery was performed at -0.8 V vs SHE to enable the reduction of elemental sulfur. Cathodic recovery was performed at potential below the hydrogen evolution potential, to achieve higher coulombic efficiency and minimize any potential damage to the electrode coating. GF-Mn_2O_3, loaded with elemental sulfur prior to the recovery, was polarized at -0.8 V vs SHE for 8 hours and concentration of HS^- and other dissolved sulfur species was measured. The concentration of HS^- increased linearly over time (i.e., from 0 mM to 1.73 ± 0.01 mM after 8 hours) confirming the possibility of cathodic sulfur recovery (Figure S11). In addition to this, the gradual buildup of yellow color, typical for polysulfide solution, was observed (Figure S10). Given the difficulties associated with the polysulfide determination, the recovery efficiency could not be calculated only based on the measured concentrations of HS^-. When the recovered material was applied for HS^- removal, the sulfide removal rate was partly restored, increasing from 0.65 ± 0.03 h^{-1} to 1.1 ± 0.035 h^{-1}. The initial sulfie removal rate of 2.42 ± 0.05 h^{-1} could not be achieved due to the partial loss of the Mn_2O_3 coating (Fig. 5b). As was shown by the GF-Mn_2O_3 electrode stability tests, performed at -0.8 V vs SHE in the 9 mmol $NaNO_3$ supporting electrolyte, increase of total dissolved manganese occurred after 3 hours of polarization. Even though measured concentration represents ≤1% of the total Mn_2O_3 deposited, the duration of recovery cycles was limited to 2 hours to ensure complete GF-Mn_2O_3 electrode stability.

To investigate the impact of cathodic recovery on the GF-Mn_2O_3 electrode performance over several cycles, each application for sulfide removal at 0.4 V vs SHE was followed by a 2 hours recovery cycle at -0.8 V vs SHE (Fig. 5c). The concentration of sulfide released from the electrode in each recovery step was continuously increasing, from 0.042 ± 0.006 mM in the first cycle to 0.92 ± 0.1 mM in the fifth cycle, indicating a gradual saturation of GF-Mn_2O_3 electrode with the elemental sulfur (Figure S12) However, as can be seen from Fig. 5c, even partial recovery had a positive impact on the system performance, yielding higher sulfide removal rates compared with the cycles performed without the recovery (e.g., 1.29 ± 0.07 and 0.65 ± 0.03, respectively). In addition, these results demonstrate that the shifts between Mn valence states that could occur under cathodic polarization could be reversed back when the positive potential was applied, as the HS^- removal rates with and without the recovery are comparable during the first cycles of application.

3.4. Electro-catalytic sulfide removal in real sewage

Sulfide removal rates observed in the experiments with real sewage were significantly lower compared to the experiments performed in the supporting $NaNO_3$ electrolyte (0.94 ± 0.13 h^{-1} and 2.42 ± 0.02 h^{-1} in sewage and $NaNO_3$ supporting electrolyte, respectively). As was previously mentioned, Mn_yO_x is an excellent catalyst, that is active for different oxidation and reduction reactions, which means that other compounds can interfere and compete with sulfide ions for active sites. For instance, COD was decreased from 500 mg/L to 420 mg/L during 2 hours, indicating oxidation of organic contaminants.

The selectivity of the process was maintained, as elemental sulfur was the major final product of the treatment. However, its deposition at the surface was partial, unlike the case with the supporting electrolyte. Part of S° intermediate, produced at the electrode surface as the result of the sulfide oxidation reaction, can desorb and undergo complexation to S_8 in the bulk of the electrolyte. The complexation to S_8, that took place directly at the surface in the NaNO3 electrolyte, is the reaction controlled by the diffusion rate of sulfide to the electrode surface [30]. Taking into account the presence of other ions such as phosphate, which is known for its ability to block Mn_xO_y active sites, sulfide diffusion towards the electrode was likely impeded [56]. Therefore, part of S° intermediate, being rather unstable, was released into the electrolyte. The desorption of S_0 intermediate was only partial, as in the recovery cycle gradual increase of sulfide concentration was still observed (i.e., from 0 to 0.2 ± 0.08 mmol), indicating presence of the deposited sulfur. Lower concentration of sulfide released in the recovery cycle compared to the electrode saturated in the $NaNO_3$

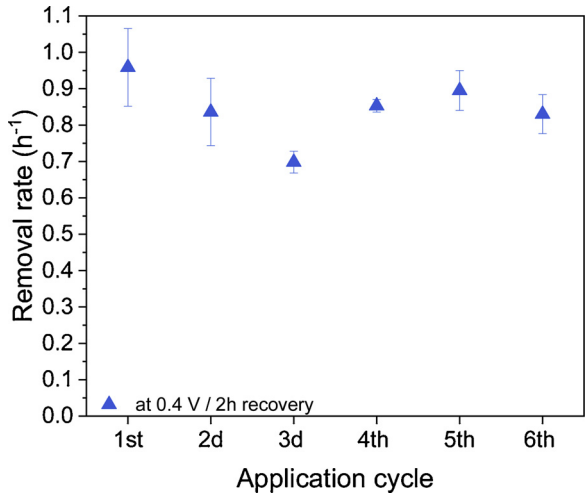

Fig. 6. Observed first-order sulfide removal rates (h^{-1}) at GF-Mn_xO_y electrodes (H-200 C, c.). applied over six subsequent cycles using real sewage.

electrolyte (0.2 ± 0.08 mmol and 0.97 ± 0.12 mmol), further confirms that less elemental sulfur was deposited.

As in the case of $NaNO_3$ electrolyte, sulfide removal from real sewage using GF-Mn_2O_3 electrode was performed over six subsequent cycles, with 2 hours cathodic recovery applied in between cycles (Fig. 6). Sulfide removal rate did not change significantly with each cycle (i.e., 0.94 ± 0.13 h^{-1} in the first cycle to 0.82 ± 0.08 h^{-1} in the sixth cycle), unlike when $NaNO_3$ supporting electrolyte was used (Fig. 5). This can be explained by a lower extent of the electrode passivation with elemental sulfur, that occurred due to the partial desorption of S_0 intermediate. Although selectivity of the process was partially lost due to the production of colloidal sulfur, it can be recovered by working in flow through mode, thus avoiding diffusion limitations and improving sulfide mass transfer towards electrode surface.

4. Conclusion

Rapid and selective sulfide oxidation to sulfur was possible using electrochemical cell equipped with Mn_xO_y coated GF electrodes. Activity of GF-Mn_xO_y electrodes synthesized via electrodeposition pathway was directly related to the active surface area of material, with lower Mn_xO_y loading yielding more relief in the coating and higher HS^- removal rates. Even though the application of low potential did not enhance sulfide oxidation, it enabled continuous regeneration of the reduced manganese after its reaction with the sulfide ion. Loss of performance due to electrode passivation with elemental sulfur was successfully slowed down by applying cathodic polarization to dissolve the deposited sulfur to HS^- and polysulfides. However, full recovery could not be accomplished to ensure the stability of the Mn_xO_y coating. Catalytic sulfide oxidation at high rates was also achieved when experiments were performed in real sewage, though, the kinetics of the oxidation was decreased by occurrence of other competing reactions.

Electrochemical recovery of Mn_xO_y, achieved in this study, is highly important as it enables continuous recovery of the catalyst that is otherwise rapidly depleted when used in a conventional homogeneous catalytic reaction. The safety and simplicity of the electrode material synthesis is an additional advantage in case of potential up scaling of the proposed technique. The selectivity of the treatment towards elemental sulfur production, that was slightly worsened in the experiments with real sewage, may be restored by working in a flow through mode and, therefore, improving the sulfide mass transfer towards the electrode surface.

N. Sergienko performed the experiments, sample analysis and wrote the manuscript. N. Sergienko and J. Radjenovic interpreted the data. J. Radjenovic designed and supervised the study.

5. Declaration of Competing Interest

The authors declare that they have no known competing financial interests or personal relationships that could have appeared to influence the work reported in this paper.

Acknowledgements

The authors would like to acknowledge ERC Starting Grant project ELECTRON4WATER (Three-dimensional nanoelectrochemical systems based on low-cost reduced graphene oxide: the next generation of water treatment systems), project number 714177.

Appendix A. Supplementary data

Supplementary material related to this article can be found, in the online version, at doi:https://doi.org/10.1016/j.apcatb.2020.118608.

References

[1] L. Zhang, P. De Schryver, B. De Gusseme, W. De Muynck, N. Boon, W. Verstraete, Chemical and biological technologies for hydrogen sulfide emission control in sewer systems: A review, Water Research 42 (2008) 1–12, https://doi.org/10.1016/j.watres.2007.07.013.
[2] A. Romanova, D.M. Mahmoodian, M. Alani, Influence and Interaction of Temperature, H2S and pH on Concrete Sewer Pipe Corrosion (2014), https://doi.org/10.5281/zenodo.1093020.
[3] I. Pikaar, E.M. Likosova, S. Freguia, J. Keller, K. Rabaey, Z. Yuan, Electrochemical Abatement of Hydrogen Sulfide from Waste Streams, Critical Reviews in Environmental Science and Technology 45 (2015) 1555–1578, https://doi.org/10.1080/10643389.2014.966419.
[4] N. Sergienko, E. Irtem, O. Gutierrez, J. Radjenovic, Electrochemical removal of sulfide on porous carbon-based flow-through electrodes, Journal of Hazardous Materials 375 (2019) 19–25, https://doi.org/10.1016/j.jhazmat.2019.04.033.
[5] K. Rankin, D. Bejan, N.J. Bunce, Electrochemical Oxidation of the Sulfide Ion in Synthetic Geothermal Brines in Batch Cells Using Coke Electrodes, Industrial & Engineering Chemistry Research 49 (2010) 6261–6266, https://doi.org/10.1021/ie901511a.
[6] J. Hastie, D. Bejan, N.J. Bunce, Oxidation of sulfide ion in synthetic geothermal brines at carbon-based anodes, The Canadian Journal of Chemical Engineering 89 (2011) 948–957, https://doi.org/10.1002/cjce.20454.
[7] B.G. Ateya, F.M. AlKharafi, A.S. Al-Azab, Electrodeposition of Sulfur from Sulfide Contaminated Brines, (2003), https://doi.org/10.1149/1.1599686.
[8] J. Dong, G. Lu, J. Yue, Z. Cheng, X. Kang, Valence modulation in hollow carbon nanosphere/manganese oxide composite for high performance supercapacitor, Applied Surface Science 480 (2019) 1116–1125, https://doi.org/10.1016/j.apsusc.2019.02.245.
[9] T. García, J.M. López, Á. Mayoral, Y. Zhang, R. Arenal, D. Alonso-Domínguez, M.P. Pico, M.L. López, A. Dejoz, I. Álvarez-Serrano, R. Sanchis, B. Solsona, Green synthesis of cavity-containing manganese oxides with superior catalytic performance in toluene oxidation, Applied Catalysis A: General 582 (2019) 117107, https://doi.org/10.1016/j.apcata.2019.06.005.
[10] J. Chen, X. Chen, D. Yan, M. Jiang, W. Xu, H. Yu, H. Jia, A facile strategy of enhancing interaction between cerium and manganese oxides for catalytic removal of gaseous organic contaminants, Applied Catalysis B: Environmental 250 (2019) 396–407, https://doi.org/10.1016/j.apcatb.2019.03.042.
[11] Y. Cheng, T. Huang, Y. Sun, X. Shi, Catalytic oxidation removal of ammonium from groundwater by manganese oxides filter: Performance and mechanisms, Chemical Engineering Journal 322 (2017) 82–89, https://doi.org/10.1016/j.cej.2017.04.010.
[12] W. Wei, X. Cui, W. Chen, D.G. Ivey, Manganese oxide-based materials as electrochemical supercapacitor electrodes, Chemical Society Reviews 40 (2011) 1697–1721, https://doi.org/10.1039/C0CS00127A.
[13] W. Xiao, P. Zhou, X. Mao, D. Wang, Ultrahigh aniline-removal capacity of hierarchically structured layered manganese oxides: trapping aniline between interlayers, Journal of Materials Chemistry A 3 (2015) 8676–8682, https://doi.org/10.1039/C5TA01305D.
[14] J. Wang, J. Li, C. Jiang, P. Zhou, P. Zhang, J. Yu, The effect of manganese vacancy in birnessite-type MnO2 on room-temperature oxidation of formaldehyde in air, Applied Catalysis B: Environmental 204 (2017) 147–155, https://doi.org/10.1016/j.apcatb.2016.11.036.
[15] J. Wang, G. Zhang, P. Zhang, Graphene-assisted photothermal effect on promoting catalytic activity of layered MnO2 for gaseous formaldehyde oxidation, Applied Catalysis B: Environmental 239 (2018) 77–85, https://doi.org/10.1016/j.apcatb.2018.08.008.
[16] A. Massa, S. Hernández, A. Lamberti, C. Galletti, N. Russo, D. Fino, Electro-oxidation of phenol over electrodeposited MnOx nanostructures and the role of a TiO2

nanotubes interlayer, Applied Catalysis B: Environmental 203 (2017) 270–281, https://doi.org/10.1016/j.apcatb.2016.10.025.
[17] Y.-q. Wang, B. Gu, W.-l. Xu, Electro-catalytic degradation of phenol on several metal-oxide anodes, Journal of Hazardous Materials 162 (2009) 1159–1164, https://doi.org/10.1016/j.jhazmat.2008.05.164.
[18] M. Nakayama, M. Shamoto, A. Kamimura, Surfactant-Induced Electrodeposition of Layered Manganese Oxide with Large Interlayer Space for Catalytic Oxidation of Phenol, Chemistry of Materials 22 (2010) 5887–5894, https://doi.org/10.1021/cm101970b.
[19] W.-c. Peng, S.-b. Wang, X.-y. Li, Shape-controlled synthesis of one-dimensional α-MnO2 nanocrystals for organic detection and pollutant degradation, Separation and Purification Technology 163 (2016) 15–22, https://doi.org/10.1016/j.seppur.2016.01.050.
[20] L. Ukrainczyk, M. McBride, Oxidation and dechlorination of chlorophenols in dilute aqueous suspensions of manganese oxides: Reaction products, Environmental Toxicology and Chemistry 12 (1993) 2015–2022, https://doi.org/10.1002/etc.5620121107.
[21] J. Qin, Q. Zhang, K.T. Chuang, Catalytic wet oxidation of p-chlorophenol over supported noble metal catalysts, Applied Catalysis B: Environmental 29 (2001) 115–123, https://doi.org/10.1016/S0926-3373(00)00200-9.
[22] Y. Wang, A. Stone, The citric acid-MnIII,IVO2(birnessite) reaction, Electron transfer, complex formation, and autocatalytic feedback, Geochimica et Cosmochimica Acta 70 (2006) 4463–4476, https://doi.org/10.1016/j.gca.2006.06.1551.
[23] Y. Wang, A. Stone, Reaction of MnIII,IV (hydr)oxides with oxalic acid, glyoxylic acid, phosphonoformic acid, and structurally-related organic compounds, Geochimica et Cosmochimica Acta 70 (2006) 4477–4490, https://doi.org/10.1016/j.gca.2006.06.1548.
[24] V.P. Santos, M.F.R. Pereira, J.J.M. Órfão, J.L. Figueiredo, The role of lattice oxygen on the activity of manganese oxides towards the oxidation of volatile organic compounds, Applied Catalysis B: Environmental 99 (2010) 353–363, https://doi.org/10.1016/j.apcatb.2010.07.007.
[25] S.S.T. Bastos, J.J.M. Órfão, M.M.A. Freitas, M.F.R. Pereira, J.L. Figueiredo, Manganese oxide catalysts synthesized by exotemplating for the total oxidation of ethanol, Applied Catalysis B: Environmental 93 (2009) 30–37, https://doi.org/10.1016/j.apcatb.2009.09.009.
[26] X. Huang, T. Chen, X. Zou, M. Zhu, D. Chen, M. Pan, The Adsorption of Cd(II) on Manganese Oxide Investigated by Batch and Modeling Techniques, Int J Environ Res Public Health 14 (2017) 1145, https://doi.org/10.3390/ijerph14101145.
[27] S.A. Chaudhry, T.A. Khan, I. Ali, Adsorptive removal of Pb(II) and Zn(II) from water onto manganese oxide-coated sand: Isotherm, thermodynamic and kinetic studies, Egyptian Journal of Basic and Applied Sciences 3 (2016) 287–300, https://doi.org/10.1016/j.ejbas.2016.06.002.
[28] R. Han, W. Zou, Z. Zhang, J. Shi, J. Yang, Removal of copper(II) and lead(II) from aqueous solution by manganese oxide coated sand I. Characterization and kinetic study, J Hazard Mater 137 (2006) 384–395, https://doi.org/10.1016/j.jhazmat.2006.02.021.
[29] R.C. Aller, P.D. Rude, Complete oxidation of solid phase sulfides by manganese and bacteria in anoxic marine sediments, Geochimica et Cosmochimica Acta 52 (1988) 751–765, https://doi.org/10.1016/0016-7037(88)90335-3.
[30] J. Herszage, M. Dos Santos Afonso, Mechanism of Hydrogen Sulfide Oxidation by Manganese(IV) Oxide in Aqueous Solutions, Langmuir 19 (2003), https://doi.org/10.1021/la034016p.
[31] K. Wlodarchak, D. Skutt, G. Deshinsky, A. Chan, E. Pedersen, Odor Reduction in a Wastewater Treatment Plant Using Potassium Permanganate, Proceedings of the Water Environment Federation 2002 (2002) 72–81, https://doi.org/10.2175/193864702785139999.
[32] F. Cadena, R.W. Peters, Evaluation of Chemical Oxidizers for Hydrogen Sulfide Control, Journal (Water Pollution Control Federation) 60 (1988) 1259–1263, https://doi.org/10.2307/25043633.
[33] S. Asaoka, H. Okamura, Y. Akita, K. Nakano, K. Nakamoto, K. Hino, T. Saito, S. Hayakawa, M. Katayama, Y. Inada, Regeneration of manganese oxide as adsorption sites for hydrogen sulfide on granulated coal ash, Chemical Engineering Journal 254 (2014) 531–537, https://doi.org/10.1016/j.cej.2014.06.005.
[34] D. Patil, S. Chavan, J.U. Kennedy Oubagaranadin, A review of technologies for manganese removal from wastewaters, Journal of Environmental Chemical Engineering 4 (2015), https://doi.org/10.1016/j.jece.2015.11.028.
[35] C. Hu, F. Liu, H. Lan, H. Liu, J. Qu, Preparation of a manganese dioxide/carbon fiber electrode for electrosorptive removal of copper ions from water, Journal of Colloid and Interface Science 446 (2015) 359–365, https://doi.org/10.1016/j.jcis.2014.12.051.
[36] H.-Q. Wang, G.-f. Yang, Q.-Y. Li, X.-X. Zhong, F.-P. Wang, Z.-S. Li, Y.-h. Li, Porous Nano-MnO2: Large Scale Synthesis Via a Facile Quick-Redox Procedure and Application in a Supercapacitor, New J. Chem. 35 (2011) 469–475, https://doi.org/10.1039/C0NJ00712A.
[37] Y. Xu, H. Lin, Y. Li, H. Zhang, The mechanism and efficiency of MnO2 activated persulfate process coupled with electrolysis, Science of The Total Environment 609 (2017) 644–654, https://doi.org/10.1016/j.scitotenv.2017.07.151.
[38] C. Zhao, X. Lv, J. Li, T. Xie, Y. Qi, W. Chen, Manganese Oxide Nanoparticles Decorated Ordered Mesoporous Carbon Electrode for Capacitive Deionization of Brackish Water, Journal of The Electrochemical Society 164 (2017) E505–E511, https://doi.org/10.1149/2.0141714jes.
[39] S. Ziller, J. Fold von Bülow, S. Dahl, M. Lindén, A fast sol-gel synthesis leading to highly crystalline birnessite under non-hydrothermal conditions, Dalton Trans. 46 (2017), https://doi.org/10.1039/C7DT00109F.
[40] X.Q. Yu, Y. He, J.P. Sun, K. Tang, H. Li, L.Q. Chen, X.J. Huang, Nanocrystalline MnO thin film anode for lithium ion batteries with low overpotential, Electrochemistry Communications 11 (2009) 791–794, https://doi.org/10.1016/j.elecom.2009.01.040.
[41] X.-W. Liu, X.-F. Sun, Y.-X. Huang, G.-P. Sheng, K. Zhou, R.J. Zeng, F. Dong, S.-G. Wang, A.-W. Xu, Z.-H. Tong, H.-Q. Yu, Nano-structured manganese oxide as a cathodic catalyst for enhanced oxygen reduction in a microbial fuel cell fed with a synthetic wastewater, Water Research 44 (2010) 5298–5305, https://doi.org/10.1016/j.watres.2010.06.065.
[42] P. Hosseini-Benhangi, C.H. Kung, A. Alfantazi, E. Gyenge, Controlling the Interfacial Environment in the Electrosynthesis of MnOx Nanostructures for High Performance Oxygen Reduction/Evolution Electrocatalysis, ACS Applied Materials & Interfaces 9 (2017), https://doi.org/10.1021/acsami.7b05501.
[43] P.K. Dutta, R.A. Rozendal, Z. Yuan, K. Rabaey, J. Keller, Electrochemical regeneration of sulfur loaded electrodes, (2009), https://doi.org/10.1016/j.elecom.2009.05.024.
[44] A. Kamyshny, I. Ekeltchik, J. Gun, O. Lev, Method for the Determination of Inorganic Polysulfide Distribution in Aquatic Systems, Analytical Chemistry 78 (2006) 2631–2639, https://doi.org/10.1021/ac051854a.
[45] W.E. Kleinjan, A.d. Keizer, A.J.H. Janssen, Kinetics of the chemical oxidation of polysulfide anions in aqueous solution, Water Research 39 (2005) 4093–4100, https://doi.org/10.1016/j.watres.2005.08.006.
[46] M.I. Zaki, M.A. Hasan, L. Pasupulety, K. Kumari, Thermochemistry of manganese oxides in reactive gas atmospheres: Probing redox compositions in the decomposition course MnO2 → MnO, Thermochimica Acta 303 (1997) 171–181, https://doi.org/10.1016/S0040-6031(97)00258-X.
[47] M. Chigane, M. Ishikawa, Manganese Oxide Thin Film Preparation by Potentiostatic Electrolyses and Electrochromism, Journal of The Electrochemical Society - J ELECTROCHEM SOC 147 (2000), https://doi.org/10.1149/1.1393515.
[48] L. Zhong Zhao, V. Young, XPS studies of carbon supported films formed by the resistive deposition of manganese, Journal of Electron Spectroscopy and Related Phenomena 34 (1984) 45–54, https://doi.org/10.1016/0368-2048(84)80058-4.
[49] B. Babakhani, D.G. Ivey, Effect of electrodeposition conditions on the electrochemical capacitive behavior of synthesized manganese oxide electrodes, Journal of Power Sources 196 (2011) 10762–10774, https://doi.org/10.1016/j.jpowsour.2011.08.102.
[50] Z.B. Jildeh, J. Oberländer, P. Kirchner, P.H. Wagner, M.J. Schöning, Thermocatalytic Behavior of Manganese (IV) Oxide as Nanoporous Material on the Dissociation of a Gas Mixture Containing Hydrogen Peroxide, Nanomaterials (Basel) 8 (2018) 262, https://doi.org/10.3390/nano8040262.
[51] M. Dupont, S. Donne, Nucleation and Growth of Electrodeposited Manganese Dioxide for Electrochemical Capacitors, (2014), https://doi.org/10.1016/j.electacta.2013.12.014.
[52] J.E. Kostka, G.W. Luther, K.H. Nealson, Chemical and biological reduction of Mn (III)-pyrophosphate complexes: Potential importance of dissolved Mn (III) as an environmental oxidant, Geochimica et Cosmochimica Acta 59 (1995) 885–894, https://doi.org/10.1016/0016-7037(95)00007-0.
[53] Comprehensive Coordination Chemistry II: From Biology to Nanotechnology. Volumes 1 – 10 Edited by Jon A. McCleverty (University of Bristol) and Thomas J. Meyer (Los Alamos National Laboratory). Elsevier: Amsterdam. 2003. ca. 7000 pp. $5975.00. ISBN 0-08-043748-6, Journal of the American Chemical Society, 126 (2004) 1922-1922 10.1021/ja033635h.
[54] B.G. Ateya, F.M. AlKharafi, A.S. Alazab, A. Abdullah, Kinetics of the Electrochemical Deposition of Sulfur from Sulfide Polluted Brines, (2007), https://doi.org/10.1007/s10800-006-9270-4.
[55] P.K. Dutta, R.A. Rozendal, Z. Yuan, K. Rabaey, J. Keller, Electrochemical regeneration of sulfur loaded electrodes, Electrochemistry Communications 11 (2009) 1437–1440, https://doi.org/10.1016/j.elecom.2009.05.024.
[56] W. Yao, F.J. Millero, The rate of sulfide oxidation by δMnO2 in seawater, Geochimica et Cosmochimica Acta 57 (1993) 3359–3365, https://doi.org/10.1016/0016-7037(93)90544-7.